Coupling meteorological variables with Moderate Resolution Imaging Spectroradiometer atmospheric products for estimating global solar radiation

Coupling meteorological variables with Moderate Resolution Imaging Spectroradiometer atmospheric products for estimating global solar radiation

Ji-Long Chen [a], L He [b], Hong Yang [c, d], Qiao Chen [a], Maohua Ma [a], Xiao-Xiao Wang[a], Zuo-lin Xiao [e],*

[a] Key Laboratory on Water Environment of Reservoir Watershed, Chongqing Institute of Green and Intelligent Technology, Chinese Academy of Sciences, Chongqing 401122, China

[b] Key Laboratory of Poyang Lake Wetland and Watershed Research, Ministry of Education, Nanchang 330000, China

[c] Collaborative Innovation Center of Atmospheric Environment and Equipment Technology, Jiangsu Key Laboratory of Atmospheric Environment Monitoring and Pollution Control (AEMPC), School of Environmental Science and Engineering, Nanjing University of Information Science & Technology, Nanjing 210044, China

[d] Department of Geography and Environmental Science, University of Reading, Reading, Whiteknights, RG6 6AB, UK

[e] The Key Laboratory of GIS Application Research, Chongqing Normal University, Chongqing 401331, China

*Corresponding author:

Dr. Zuo-lin Xiao

The Key Laboratory of GIS Application Research

Chongqing Normal University, Chongqing 401331, China

Tel.: +86 023 6593 5878

Email address: xiaoll@cqnu.edu.cn

Abstract: Global solar radiation is a crucial variable for scientific researches and solar energy application, while it is measured at very few sites mainly due to the technical and fiscal obstacles. Developing robust and accurate models for estimating global solar radiation had been being a focus for many studies. This study was conducted to develop integrated models combining Moderate Resolution Imaging Spectroradiometer atmospheric products and meteorological variables. 43 empirical models based on the meteorological variables were collected. A total of 645 integrated models incorporating atmospheric constituents into the empirical models were developed. The researched models were evaluated and compared at Chongqing in Three Gorges Reservoir Area, China. The results showed that the integrated models outperformed the empirical models. The best integrated model had the root mean square error of 0.817 MJ m^{-2} and relative root mean square error of 8.11%. On average, the integrated models had the root mean square error of 1.071 MJ m^{-2}, 15.6% smaller than the empirical models. The results suggest that coupling Moderate Resolution Imaging Spectroradiometer atmospheric products with meteorological variables can enhance the performance of the conventional empirical models, which may provide a promising alternative to generate global solar radiation data with better accuracy.

Keywords: Global solar radiation, Moderate Resolution Imaging Spectroradiometer, empirical models, meteorological variables

1 Introduction

Solar radiation arriving at the earth's surface plays an important role in maintaining physical [1], biological [2] and chemical processes on the earth [3]. It is an essential variable for scientific researches in climate [4], ecology [5] and agriculture [6], as well as a crucial parameter for engineering applications in designing solar furnaces [7], sizing photovoltaic cells [8] and developing efficient solar energy system [9]. However, solar radiation data are not easily available mainly due to the equipment [10], measuring manipulation [11] and financial limitations [12]. As the result, great efforts have been made to estimate global solar radiation from other commonly measured meteorological variables such as air temperature [13] and sunshine duration [14]. Due to the simplicity and operability yet reasonable accuracy, empirical model is the most widely employed approach [15].

Many empirical models have been developed in literatures among which the earliest ones were proposed by Angstrom [16] and Prescott [17]. They correlated clearness index (ratio of global solar radiation to extraterrestrial radiation) with sunshine fraction (the ratio of sunshine duration to potential sunshine duration) and developed the Angstrom-Prescott (A-P) model. This model was revised by many researchers. For example, Almorox and Hontoria [18] developed an exponential model for Spain; Ampratwum and Dorvlo [19] proposed a logarithmic equation for arid region in Oman; Ogelman et al. [20] suggested a quadratic function for Turkey. Bahel et al. [21] proposed a cubic model based on the data of 48 stations around the world. Newland [22] modified the A-P model and proposed a linear logarithmic model. However, many comparative studies suggested that those revisions did not improve the estimation. For example, Chen et al. [23] evaluated the accuracy of 28 sunshine-based models and reported that revision of the A-P model by changing the structure from linear to nonlinear were generally ineffective. Yorukoglu and Celik [24] investigated the performances of linear, quadratic, cubic, logarithmic and exponential models, and the results showed that those models returned similar error

indicators at Ankara in Turkey. Zhou et al. [25] assessed the precision of several sunshine-based models and found that the A-P model performed similarly to its revisions in China. Consequently, air temperature [26], relatively humidity [27], precipitation [28], atmospheric pressure and vapor pressure [29] were incorporated. Comparisons and evaluations showed that these modifications enhanced the accuracy of the A-P models. Chen and Li [30] calibrated 9 sunshine-based models and the comparisons showed that the modification to A-P model by introducing air temperature decreased the estimation error of the A-P model. Falayi et al. [31] observed that the combination of sunshine duration, temperature and relative humidity yielded better precision than other models in Nigeria. Ouali and Alkama [32] evaluated the performances of 4 models and reported that inclusion of precipitation and wind velocity increased the accuracy of the models employing sunshine fraction in Nigeria.

The sunshine-based models were widely used because of their promising performances. However, they are limited to the sites with available sunshine data [33]. Therefore, Hargreaves and Samani [34] proposed a simple function (H-S model) of air temperature. Bristow and Campbell [35] also developed an exponential model (B-C model) using temperature range. Both models were widely modified and validated, and the evaluations showed that the performances of H-S and B-C models and their modifications varied from regions to regions, and the accuracies were affected by the geographic location and local climate [36]. For example, Hunt et al. [37] introduced precipitation in an additive form that significantly outperformed the H-S model at 8 sites in Canada. Thornton and Running [38] modified the B-C model and presented a new formulation using temperature, relative humidity and atmospheric pressure. Evaluation showed that the new model outperformed that B-C model at 40 stations in the USA, while this new model gave similar estimation to the H-S model in North America [39].

Although great efforts have been conducted and a large number of empirical models had been

developed since the pioneering works of Angstrom [16] and Prescott [17]. It is still difficult to develop more robust and accuracy models due to the complex process of radiation [40]. Evaluations and comparative studies indicated that empirical models employing the meteorological variables have overreached their predictive limits [41]. Besides, the empirical models based on meteorological measurements at point scale are insufficient for the application at regional scale [42], particularly for the large, remote areas where measurements of climatological variables are difficult [43].

Solar radiation is attenuated mainly by cloud, aerosol, and water vapor on its way through the atmosphere [42]. The impact of cloud on solar radiation is more pronounced than those by other atmospheric constituents [44]. Because a large part of radiation is reflected back to space by cloud, beam radiation can decrease to a level at 0 MJ m^{-2} [45]. Aerosol mainly scatters shortwave radiation in forward direction [46]. Water vapor contributes little in absorbing near-infrared radiation but significantly in budgeting the heat in the lower atmosphere [47]. These atmospheric constituents can be detected at large spatial and temporal scales with satellite observation, which overcomes the limitations of site measurements and provides an opportunity to enhance the performances of the empirical models by incorporating satellite observation with ground measurements of climatological variables.

MODIS (Moderate Resolution Imaging Spectroradiometer) is a key sensor operated on both the Terra and Aqua satellites. Its detectors can measure 36 spectral bands between 0.41 and 14.39μm [42]. Many products derived from MODIS observations deliver featured information that can be used for studies of global dynamics and processes involving in land, oceans, and the lower atmosphere. Among these products, MODIS aerosol products (MOD04) monitor the properties of the aerosol over land and ocean surfaces [48]; MODIS precipitable water product (MOD05) consists of column water-vapor amounts [49]; MODIS cloud product (MOD06) combines infrared emission and solar reflectance techniques for determining both physical and radiative cloud properties [50]. These datasets played an important role in

understanding of atmosphere dynamics and the land-atmosphere interactions. Moreover, MODIS products are widely available for free.

Thus, estimations of solar radiation employing the MODIS data have recently been investigated. Performances of four machine learning algorithms integrated with MODIS datasets were evaluated in Australia [51], showing that those algorithms integrated with MODIS data can be applied as a qualified tool in data-sparse regions. After investigating the precision of artificial neural network using MODIS data in Queensland, Ravinesh and Mehmet [52] confirmed that this algorithm coupled with MODIS data was a powerful stratagem. The random forest approach using MODIS data was applied in the USA [53], indicating that the model simulations matched well with the observations. A comparative study of four models was conducted in China [54], and results showed that those models with MODIS data can be used to reveal the spatial-temporal variations of solar radiation at large scale. Considering atmosphere as homogeneous and plane-parallel layers without three-dimensional effects, Chen et al. [55] developed a computing scheme using MODIS atmospheric products based on radiative transfer processes. Although evaluations showed good agreement between the estimations and observations, the rigorous radiative transfer algorithms are too complicated, data-intensive and time-consuming to be handled by users in other areas. Therefore, a simple model with reasonable accuracy using MODIS atmospheric products across China was proposed by Chen et al. [42].

Due to the optimum trade-off between simplicity and accuracy, empirical model employing the meteorological variables is the most common approach for estimating solar radiation at point scale. Recent studies suggested that MODIS data can be used to obtain solar radiation data, particularly for the data sparse and remote areas. Moreover, it can be used to retrieve the spatial distribution of radiation at large scale. It is therefore open to question whether and to what extent the performance of the empirical model can be enhanced by combining the meteorological variables with MODIS atmospheric products.

With respect to the advantages of MODIS data and the empirical approach, estimation of global solar radiation coupling MODIS data with meteorological variables was investigated in this study. The main objectives of this study are to (1) collect the widely used empirical models employing different combinations of meteorological variables, (2) develop integrated empirical models by coupling meteorological variables with MODIS atmospheric products, and (3) evaluate and compare the presently developed models against the empirical models in the Three Gorges Reservoir Area (TGRA), China.

2 Materials and methods

This section provides the details about the collected empirical models, the process of the integrated models developments, the evaluation and validation indicators, the research site, data collection and processing of MODIS atmospheric products and meteorological datasets.

2.1 Empirical models

In order to verify the performances of the newly developed models, a total of 43 widely used empirical models employing different combinations of meteorological variables were collected and evaluated. Among them, 25 models (models 1-25) were reported for the sunshine-based models, and 18 models (models 26-43) for the temperature-based models.

Model 1: Angstrom [16] developed a simple correlation between the ratio of global radiation to the radiation on a clear day and sunshine fraction. Replacing the radiation on a clear day with the extraterrestrial radiation, Prescott [17] revised the Angstrom model and proposed the following model:

$$\text{Model 1:}\quad Rs/Ra = aS/So + b \tag{1}$$

where a and b are empirical coefficients; S is sunshine duration; So is potential sunshine duration; Rs is global solar radiation; Ra is extraterrestrial radiation. Rs and Ra are calculated using the equations detailed by Allen et al [64].

$$Ra = 37.6d(\omega \sin\sin\delta + \cos\cos\delta \sin\omega) \tag{2}$$

$$d = 1 + 0.033\cos\left(\frac{2\pi}{365}n\right) \quad (3)$$

$$\delta = 0.4093\sin\left(\frac{2\pi}{365}n - 1.39\right) \quad (4)$$

$$\omega = \arccos(-\tan\varphi\tan\delta) \quad (5)$$

$$So = 24\omega/\pi \quad (6)$$

where d is the relative distance between the sun and the earth; ω is sunset hour angle (rad); φ is latitude (rad); δ is solar declination angle (rad); n is the number of the day of year starting from the first of January.

Model 2: Bakirci [57] revised the A-P model by adding an exponential term and suggested a linear exponential model.

$$\text{Model 2: } Rs/Ra = a + b_1 S/S_0 + b_2 exp(S/S_0) \quad (7)$$

Model 3: Newland [22] added a logarithmic term to the A-P model and presented a linear logarithmic model.

$$\text{Model 3: } Rs/Ra = a + b_1 S/S_0 + b_2 log(S/S_0) \quad (8)$$

Model 4: Ögelman et al. [20] proposed a quadratic model using sunshine fraction in the following form:

$$\text{Model 4: } Rs/Ra = a + b_1 S/S_0 + b_2 (S/S_0)^2 \quad (9)$$

Model 5: Bahel et al. [21] developed a cubic function of sunshine fraction.

$$\text{Model 5: } Rs/Ra = a + b_1 S/S_0 + b_2 S/S_0^2 + b_3 S/S_0^3 \quad (10)$$

Models 6-7: Falayi et al. [31] introduced temperature to modify the A-P model and reported the following models:

$$\text{Model 6: } Rs/Ra = a + b_1 S/S_0 + c_1 T \quad (11)$$

$$\text{Model 7: } Rs/Ra = a + b_1 S/S_0 + c_1 Tmin \quad (12)$$

where *T*, *Tmin* is average temperature and minimum air temperature, respectively; c_1 is empirical

coefficient.

Model 8: Olayinka [58] suggested the following model using sunshine fraction and maximum temperature:

$$\text{Model 8: } Rs/Ra = a + b_1 S/S_0 + c_1 Tmax \quad (13)$$

where $Tmax$ is maximum air temperature.

Models 9-13: Chen and Li [30] developed the following multivariate linear models combing sunshine fraction, minimum temperature, maximum temperature, precipitation, atmospheric pressure and relative humidity.

$$\text{Model 9: } Rs/Ra = a + b_1 S/S_0 + c_1 Tmin + c_2 Tmax \quad (14)$$

$$\text{Model 10: } Rs/Ra = a + b_1 S/S_0 + e_1 P \quad (15)$$

$$\text{Model 11: } Rs/Ra = a + b_1 S/S_0 + f_1 Ap \quad (16)$$

$$\text{Model 12: } Rs/Ra = a + b_1 S/S_0 + c_1 Tmin + c_2 Tmax + d_1 Rh \quad (17)$$

$$\text{Model 13: } Rs/Ra = a + b_1 S/S_0 + c_1 Tmin + c_2 Tmax + e_1 P \quad (18)$$

where P, Ap and Rh are precipitation, atmospheric pressure and relative humidity, respectively; d_1, e_1 and f_1 are empirical coefficients.

Models 14-16: Abdallah [59] presented the following models employing sunshine fraction, temperature range, average temperature and relative humidity.

$$\text{Model 14: } Rs/Ra = a + b_1 S/S_0 + c_1 \triangle T \quad (19)$$

$$\text{Model 15: } Rs/Ra = a + b_1 S/S_0 + c_1 T + d_1 Rh \quad (20)$$

$$\text{Model 16: } Rs/Ra = a + b_1 S/S_0 + c_1 \triangle T + d_1 Rh \quad (21)$$

where $\triangle T$ is air temperature range.

Model 17: Swartman and Ogunlade [60] modified the A-P model using relative humidity and proposed the following model:

Model 17: $Rs = a + b_1 S/S_0 + d_1 Rh$ (22)

Model 18: Bakirci [28] developed a new model employing sunshine fraction and relative humidity.

Model 18: $Rs/Ra = a + b_1 S/S_0 + b_2 (S/S_0)^2 + d_1 Rh$ (23)

Model 19: Al-Salihi et al. [61] suggested a multivariate linear model coupling sunshine fraction, with maximum temperature and relative humidity.

Model 19: $Rs/Ra = a + b_1 S/S_0 + c_1 Tmax + d_1 Rh$ (24)

Model 20: Chen et al. [62] modified the A-P model using average temperature and precipitation and proposed the following model:

Model 20: $Rs/Ra = a + b_1 S/S_0 + c_1 T + e_1 P$ (25)

Model 21: Okonkwo and Nwokoye [63] presented the following model combing sunshine fraction, minimum temperature and precipitation.

Model 21: $Rs/Ra = a + b_1 S/S_0 + c_1 Tmin + e_1 P$ (26)

Model 22: Kirmani et al. [64] reported a multivariate linear model employing sunshine fraction, average temperature, relative humidity and precipitation in the following form:

Model 22: $Rs/Ra = a + b_1 S/S_0 + c_1 T + d_1 Rh + e_1 P$ (27)

Model 23: Chen and Li [65] coupled the sunshine fraction with air temperature range, relative humidity and atmospheric pressure and developed a new model as follow.

Model 23: $Rs/Ra = a + b_1 S/S_0 + c_1 \triangle T^{0.5} + d_1 Rh + f_2 Ap$ (28)

Model 24: Adeala et al. [66] suggested the following function of sunshine fraction, temperature range, relative humidity and wind velocity.

Model 24: $Rs/Ra = a + b_1 S/S_0 + c_1 T + d_1 Rh + h_1 Wv$ (29)

where Wv is wind velocity, and h_1 is empirical coefficient.

Model 25: Ouali and Alkama [67] presented a multivariate linear model incorporating sunshine

fraction, average temperature, relative humidity, precipitation and wind velocity.

$$\text{Model 25: } Rs/Ra = a + b_1 S/S_0 + c_1 T + d_1 Rh + e_1 P + h_1 Wv \quad (30)$$

Model 26: Hargreaves and Samani [34] suggested a simple model using the temperature range.

$$\text{Model 26: } Rs/Ra = a + c_1(\triangle T)^{0.5} \quad (31)$$

Models 27-28: Falayi et al. [31] developed 2 simple models employing the average temperature and minimum temperature.

$$\text{Model 27: } Rs/Ra = a + c_1 T \quad (32)$$

$$\text{Model 28: } Rs/Ra = a + c_1 Tmin \quad (33)$$

Model 29: Awachie and Okeke [68] presented a linear correlation between clearness index and maximum temperature:

$$\text{Model 29: } Rs/Ra = a + c_1 Tmax \quad (34)$$

Model 30: Bristow and Campbell [35] proposed an exponential function of temperature range.

$$\text{Model 30: } Rs/Ra = c_1(1 - exp(c_2 \triangle T^{c3})) \quad (35)$$

Models 31-32: Ohunakin et al. [69] reported the following models using temperature range and average temperature:

$$\text{Model 31: } Rs/Ra = a + c_1(\triangle T)^{0.5} + c_2(\triangle T) \quad (36)$$

$$\text{Model 32: } Rs/Ra = a + c_1 T + c_2 T^2 \quad (37)$$

Models 33-34: Li et al. [70] developed 2 linear models combing maximum temperature, minimum temperature and precipitation:

$$\text{Model 33: } Rs/Ra = a + c_1 Tmax + c_2 Tmin \quad (38)$$

$$\text{Model 34: } Rs/Ra = a + c_1 Tmax + c_2 Tmin + e_1 P \quad (39)$$

Models 35-36: Okundamiya and Nzeako [71] suggested 2 quadratic models employing minimum temperature and maximum temperature.

Model 35: $Rs/Ra = a + c_1Tmin + c_2Tmin^2$ (40)

Model 36: $Rs/Ra = a + c_1Tmax + c_2Tmax^2$ (41)

Model 37: El-Sebaii et al. [72] reported a new model combing average temperature and relative humidity.

Model 37: $Rs/Ra = a + c_1T + d_1Rh$ (42)

Models 38-42: Chen and Li [30] developed 5 models coupling air temperature with relative humidity, precipitation and atmospheric pressure.

Model 38: $Rs/Ra = a + c_1\triangle T^{0.5} + d_1Rh$ (43)

Model 39: $Rs/Ra = a + c_1\triangle T^{0.5} + e_1P$ (44)

Model 40: $Rs/Ra = a + c_1\triangle T^{0.5} + f_1Ap$ (45)

Model 41: $Rs/Ra = a + c_1\triangle T^{0.5} + d_1Rh + f_1Ap$ (46)

Model 42: $Rs/Ra = a + c_1Tmax + c_2Tmin + d_1Rh + f_1Ap$ (47)

Model 43: Korachagaon and Bapat [73] suggested the following model using maximum temperature, temperature range and relative humidity.

Model 43: $Rs/Ra = a + c_1Tmax + c_2\triangle T + d_1Rh$ (48)

2.2 New model development

After a number of preliminary experimental investigations, a total of 15 models using the possible combinations of cloud fraction, cloud optical thickness, aerosol optical thickness and precipitable water vapor amount were developed (Table 1). These parameters were widely employed for satellite-based retrieval of solar irradiance [74]. Among these models, models RS1-4 used one variable only, models RS5-10 employed the possible combinations of two variables, models RS11-14 incorporated three variables of atmospheric constituent, and model RS 15 used all the selected atmospheric constituent variables.

Subsequently, the integrated models coupling the presently developed models with the collected empirical models were further developed. The possible combinations of 43 empirical models and 15 new models resulted in 645 (43×15) coupled models by incorporating the linear combination of atmospheric constituents into the empirical models in additive form. For example, integrating model RS15 into model 1 resulted in model M1RS15 as the following form:

$$Rs/Ra = a + b_1 S/S_0 + a_1 CF + a_2 COT + a_3 PWV + a_4 AOT \quad (49)$$

where CF, COT, PWV and AOT are cloud fraction, cloud optical thickness, precipitable water vapor amount and aerosol optical thickness, respectively. The part of $b_1 S/S_0$ is from the model 1, and the part of $a_1 CF + a_2 COT + a_3 PWV + a_4 AOT$ is from model RS15. Other models were developed as the same way and presented in Table 2.

2.3 Statistical evaluation and validation

Root mean square error (RMSE) and relative root mean square error (RRMSE) (%) were selected to assess the researched models. RMSE is a widely used indicator for evaluating the model performances by allowing a term-by-term comparison of the estimation and measurements. RRMSE is a relative error indicator allowing comparisons among a range of different models. Lower RMSE and RRMSE mean better performances. RMSE and RRMSE were calculated using the following equations:

$$RMSE = \sqrt{\frac{\sum_{i=1}^{n}(y_{i,m} - y_{i,p})^2}{n}} \quad (50) \qquad RRMSE(\%) = 100\sqrt{\frac{\sum_{i=1}^{n}(y_{i,m} - y_{i,p})^2}{n y_{i,m}}} \quad (51)$$

where n, $y_{i,m}$, and $y_{i,p}$ are the number of validating record, the measurements and the estimations, respectively.

2.4 Research site

The researched models were evaluated and compared at the Chongqing meteorological station in the upper section of TGRA in China (29° 35′ N, 106° 28′ E), with the elevation of 259.1m above the sea

level. Chongqing is in the subtropical monsoon climate zone with a hot and humid summer and a cool winter [75]. Figure 1 shows the temporal variation of meteorological variables at the research site. Monthly sunshine duration ranged from the maximum in July to the minimum in December, with the average of 2.73h (Fig.1a). Monthly precipitation ranged from the maximum in June and the minimum in December, with the annul amount of 1099 mm (Fig.1a). Maximum, average and minimum temperatures presented the similar temporal variations with the highest peak in July and lowest in January (Fig.1b). Atmospheric pressure showed opposite pattern to temperatures and precipitation (Fig.1c). The average relative humidity and wind velocity were 77.01% and 1.24m/s (Fig.1d), respectively, without clear temporal patterns.

2.5 Data collection

The MODIS atmospheric products covering the period from March 2000 to December 2016 were obtained from the Earth Observing System Data and Information System (EOSDIS) of National Aeronautics and Space Administration (NASA) (https://earthdata.nasa.gov/). Cloud fraction and cloud optical thickness were extracted from MOD06. Cloud fraction was produced by infrared-only retrieval methods, and cloud optical thickness was retrieved from visible and near-infrared channels [76]. Aerosol optical thickness was extracted from MOD04 and was derived using MODIS channels 1 through 7, cloud mask product and meteorological data [42]. Precipitable water vapor amount was extracted from MOD05 and was generated by using a near-infrared algorithm [77].

Meteorological data covering the same period with MODIS data were obtained from the National Meteorological Information Center (NMIC), China Meteorological Administration (CMA). Global solar radiation (MJ m^{-2}) was measured using Pyranometer (5%) [78]. The type of Pyranometer used by the CMA was changed in 1993 [79]. However, the homogeneity of the radiation data was probably little affected because these instruments have been calibrated to the same standard following the guidelines of

the World Meteorological Organization (WMO) [40]. The assumed homogeneity was also implied by a similar trend of the Chinese radiation data series [79] to those from other places [80]. Sunshine duration (h), air temperatures (°C), atmospheric pressure (Kpa), and relative humidity (%) were measured using Jordan sunshine recorder, Mercury alcohol thermometers, Mercury barometer, and Aspirated psychomotor at 2m height, respectively [40]. Wind velocity (m/s) was measured using EL wind electric anemometer at 10m height, which was transformed to speed at 2m height by the method proposed by FAO56 [56]. All the equipment and sensors were checked and calibrated periodically, and all the measurements were made following the procedures recommended by the WMO [79].

2.6 Data check and processing

Although the quality of meteorological data has been checked by the NMIC. Meteorological records probably still contain errors associated with the manipulations, sensors errors and occasional voltage instability [81]. Therefore, the quality control scheme suggested by Feng et al. [82] and Tang et al. [83] was adopted to further check the data. Firstly, the records with missing data labeled by the feature values were removed. Secondly, the data with evident systematic errors were removed. Finally, a multivariate regression relationship between global radiation and meteorological variables was built to exclude noisy data and suspected data. More details can be referred to Feng et al. [82] and Tang et al. [83]. For the MODIS atmospheric constituent dataset, the records with missing value filled by 9999 were excluded from the dataset.

Each record of atmospheric constituents and meteorological data was identified uniquely by the year and month. Thus, an integrated dataset combining the meteorological data with the corresponding atmospheric constituent data was subsequently built by the unique identification. The records with missing data of atmospheric constituent data or meteorological data were further removed. Then two sub-datasets were built; the first 75% of the records were used for modelling and calibration, and the

344 remaining 25% for evaluation and validation.

345 3. Results and discussion

346 The performances of the researched models were presented in Table 1 and Tables 3-5. The calibrated
347 coefficients of the models were presented in supplementary data. All the collected empirical models
348 (models 1-43) performed well with the average RMSE of 1.269 MJ m^{-2} and the average RRMSE of
349 12.58%. Model 25 was the most accurate one with the lowest RMSE of 0.967 MJ m^{-2} and the RRMSE
350 of 9.58%, while the error indicators were similar to models 12, 13, 15, 22 and 24. Overall, the
351 sunshine-based models (models 1-25) had the average RMSE of 1.051 MJ m^{-2} and the average RRMSE
352 of 10.41%, which were lower than 1.574 MJ m^{-2} and 15.61%, respectively, for the temperature-based
353 models (models 26-43), suggesting that the sunshine-based models were superior to the
354 temperature-based models. This confirmed the results of previous studies. For example, Chen et al. [23]
355 evaluated the performances of 273 sunshine-based and temperature-based models and the results
356 suggested that the sunshine-based models are generally more accurate than the temperature-based
357 models in China. Besharat et al [84] comprehensively reviewed 78 empirical models, and the evaluation
358 showed that the sunshine-based models outperformed the temperature-based models in Iran.

359 Models 2-5 are the revisions of the A-P model by changing the structure from linear to nonlinear
360 forms. Models 1-5 had very similar estimations, indicating that such revisions by changing the structure
361 from linear to nonlinear were generally ineffective and yielded little improvement. This agreed well with
362 previous conclusions from Yorukoglu and Celik [24], Zhou et al. [25] and Chen et al [6] who
363 investigated and compared the performances of sunshine-based models, and reported that the revised
364 versions of A-P model, including the linear exponential, linger logarithm, quadratic and cubic models,
365 performed similar to the A-P model. Only a few works reported better performances. For instance,
366 Bakirci [28] evaluated some sunshine duration models and observed that the linear exponential

performed best in different regions of Turkey. Newland [22] found that the linear logarithmic function showed better estimation than the A-P model in South China.

Models 6-9 and 14, modified from the A-P model by introducing air temperatures, had lower estimation errors than the A-P model and models 2-5, indicating that inclusion of air temperatures enhanced the performances of the sunshine duration models. This was further proved by the better performances of models 12, 15, 16 and 19 than the model 17, and lower estimation errors of models 13, 20 and 21 than the model 10. The results were consistent with those from Khil-Ha Lee [26], Chen et al. [85] and Boluwaji and Onyedi [86] who found the models incorporating sunshine duration and air temperatures provided better estimations than the sunshine duration models. While Wu et al. [87] reported that modification from the A-P model by introducing air temperature performed similarly to the A-P model in China.

Models 17 and 18 were modifications to sunshine duration models by introducing relative humidity, and models 10 and 11 were modifications from the A-P model using precipitation and atmospheric pressure, respectively. Models 10, 17 and 18 performed similarly to models 1-5, indicating that inclusions of relative humidity and precipitation did not improve the estimation of the sunshine duration models. This was also demonstrated by the similar performances of models 13, 16, 20, 21 and 22 to the corresponding models 6, 7, 9, 14 and 15. These results were in agreement with Meenal [88] who evaluated 16 empirical models and found the exclusion of relative humidity did not affect the accuracy of sunshine duration models. Chen and Li [30], and Chen et al. [62] also observed that modifications to the A-P model using relative humidity and precipitation had the similar estimations with the A-P model. Model 11 showed lower RMSE and RRMSE than the models 1-5, suggesting that inclusion of atmospheric pressure decreased the estimation error of the sunshine duration models. The result was different from that of Chen and Li [30] who reported that atmospheric pressure did not contribute to the

improvement in estimating accuracy of the A-P model.

When sunshine duration data were unavailable, the temperature-based models (models 26-43) generated reasonable estimations with the average RMSE of 1.574 MJ m^{-2} and average RRMSE of 15.61%. Model 42 gave the best estimation with the lowest RMSE of 1.154 MJ m^{-2} and the RRMSE of 11.44%, followed by model 43 with similar error indicators to model 42.

Models 27-29, 32, 35 and 36 only using average or maximum or minimum temperature had the average RMSE of 1.875 MJ m^{-2} and average RRMSE of 18.59%, which were relatively higher than other temperature-based models. The poor performances of these models had also been reported by Chen et al. [89] who claimed that the models using temperature only were unsuitable for estimating solar radiation in China. The average RMSE and RRMSE decreased to 1.519 MJ m^{-2} and 15.07%, respectively, for models 26, 30, 31 and 33 which used the combination of maximum and minimum temperatures. The B-C model (model 30) and model 31 had similar estimations, which were slight better than the H-S model (model 26).

Model 37 using relative humidity and average temperature showed much lower RMSE and RRMSE than model 27, suggesting that inclusion of relative humidity increased the estimating accuracy of the models only using air temperature. This was further confirmed by the better performances of models 38 and 43 over the corresponding models 27 and 29.

Model 40 using atmospheric pressure and temperature range outperformed model 26, suggesting that modifications to the H-S models by introducing atmospheric pressure can enhance its performance. This was also indicated by the lower estimation errors of model 41 than model 38. These results agreed well with the findings of Chen and Li [30] who founded the additional inclusion of atmospheric pressure and relative humidity decreased the estimating errors of the temperature models. Model 39 performed similarly to the H-S model, indicating that inclusion of the precipitation as an additive form hardly

improved its accuracy, whereas Ouali and Alkama [67] discovered that the application of precipitation enhanced the performance of temperature models in Algeria.

Among the models (models RS1-15) using atmospheric constituents, model RS15 using all the atmospheric constituents had the lowest RMSE of 1.267 MJ m^{-2} and the lowest RRMSE of 12.56%, which were very similar to the corresponding values of 1.269 MJ m^{-2} and 12.58% for the model RS12 using cloud fraction, cloud optical thickness and precipitable water vapor amount. Models RS2-4, 8 and 10 showed higher estimating errors than other modes. It was generally recognized that cloud cover was the most important factor attenuating solar radiation [42]. However, the model RS1 only using cloud fraction explained 61% of the solar radiation variance (supplement data). The result confirmed the previous finding that dependence of global solar radiation on cloud was not entirely deterministic [90]. The estimation errors of models RS5 and RS7 were much lower than model RS1, suggesting that inclusion of cloud optical thickness and precipitable water vapor amount markedly increased the estimating accuracy of the models only using cloud fraction. This was also proved by the better performances of models RS 11-13 than model RS1. While model RS6 generated similar estimation with model RS1, generally implying that aerosol optical thickness did not contribute to the improvement in estimating accuracy. The results confirmed the previous findings over China [42].

All the integrated models combining the meteorological variables and atmospheric constituents showed good performances with the average RMSE of 1.071 MJ m^{-2} and the RRMSE of 10.62%, which were lower than the corresponding values of 1.269 MJ m^{-2} and 12.58% for the empirical models 1-43, suggesting that incorporation of atmospheric constituents enhanced the performance of empirical models employing meteorological variables. The models (16^{th} column in Tale 2 and Table 4-5) using the meteorological variables and all the atmospheric constituents had the lowest average RMSE of 0.929 MJ m^{-2} and the RRMSE of 9.22% and they performed similarly to the models (13^{th} column Tale 2 and Table

436 4-5) using the meteorological variables and cloud fraction, cloud optical thickness and precipitable water
437 vapor amount. Amongst all the integrated models, the model M25RS15 performed best with the lowest
438 RMSE of 0.817 MJ m^{-2} and the RRMSE of 8.11%.

439 Models M1RS2-M25RS2 had the average RMSE of 0.938 MJ m^{-2}, which was 10.63% lower than the
440 models 1-25, suggesting that incorporation of cloud optical thickness into the sunshine-based models
441 improved their estimations. The average RMSE of models M1RS1-M25RS1, M1RS3-M25RS3, and
442 M1RS4-M25RS4 were 1.016 MJ m^{-2}, 1.045 MJ m^{-2}, and 1.017 MJ m^{-2}, respectively, which were very
443 similar to 1.051 MJ m^{-2} for models 1-25. This implied that additional inclusions of cloud fraction,
444 aerosol optical depth, and precipitable water vapor amount to the sunshine-based models yielded little
445 improvement. The reason for lack of improvement may be that the potential effects of those additional
446 variables had already been implicitly reflected in the sunshine-based models. The other reason may lie in
447 the inter-dependency of different variables [6].

448 Models M1RS5-M25RS5, M1RS8-M25RS8, and M1RS9-M25RS9 performed better than models
449 1-25 with an average of 14.72%, 10.88%, and 13.99% lower RMSE, respectively. Models
450 M1RS11-M25RS11, M1RS12-M25RS12, and M1RS14-M25RS14 outperformed models 1-25 with an
451 average of 14.99%, 18.12%, and 13.84% higher accuracy, respectively. While models M1RS7-M25RS7,
452 and M1RS10-M25RS10 generated similar estimations to models 1-25. These results further indicated
453 that combining the cloud optical thickness and meteorological variables enhanced the performance of
454 the sunshine-based models, while incorporations of cloud fraction, aerosol optical depth, and
455 precipitable water vapor amount accounted less for the improvement in estimation accuracy.

456 In the case that sunshine duration data were unavailable, the integrated models combining the
457 meteorological variables and the atmospheric constituents had the average RMSE of 1.242 MJ m^{-2} and
458 the average RRMSE of 12.31%, which were lower than the corresponding values of 1.574 MJ m^{-2} and

459 average RRMSE of 15.61% for models 26-43, suggesting that incorporation of atmospheric constituents
460 into the temperature-based models improved the estimation accuracy. Overall, model M42RS15
461 generated the best estimations with the lowest RMSE of 0.903 MJ m^{-2} and the RRMSE of 8.95%.

462 Models M26RS1-M43RS1, M26RS2-M43RS2, and M26RS4-M43RS4 had the average RMSE of
463 1.282MJ m^{-2}, 1.388 MJ m^{-2}, and 1.414 MJ m^{-2}, respectively, which were lower than 1.574 MJ m^{-2} for
464 models 26-43. This suggested that combining the cloud fraction, cloud optical thickness, and
465 precipitable water vapor amount and meteorological variables increased the estimation accuracy of the
466 temperature-based models, which was further indicated by the better performances of models
467 M26RS5-M43RS5, M26RS7-M43RS7, M26RS9-M43RS9, and M26RS12-M43RS12 over models
468 26-43. The improvement was more pronounced for incorporation of cloud fraction which decreased the
469 RMSE of models 26-43 by 17.65%. Models M26RS3-M43RS3 performed similarly to models 26-43,
470 implying that inclusion of aerosol optical depth did not markedly affect the performances of the
471 temperature-based models. The similar performances of models M26RS6-M43RS6, M26RS8-M43RS8,
472 and M26RS10-M43RS10 to the corresponding models M26RS1-M43RS1, M26RS2-M43RS2, and
473 M26RS4-M43RS4 further confirmed this result.

474 4 Concluding remarks

475 This study coupled the meteorological variables with the MODIS atmospheric products to estimate
476 global solar radiation. 25 sunshine-based empirical models and 18 temperature-based empirical models
477 were collected. A total of 645 coupled models incorporating cloud fraction, cloud optical depth, aerosol
478 optical depth and precipitable water vapor amount into those empirical models were developed. The
479 researched models were evaluated and compared at Chongqing in the Three Gorges Reservoir Area in
480 China. The results suggested that the coupled models markedly outperformed the sunshine-based and
481 temperature-based models, and incorporation of atmospheric constituents enhanced the performance of

empirical models. The average RMSE decreased from 1.269 MJ m^{-2} for the empirical models to 1.071 MJ m^{-2} for the coupled models. Overall, the model incorporating atmospheric constituents into the model proposed by Ouali and Alkama [67] generated the best estimation with the lowest RMSE of 0.817 MJ m^{-2} and the RRMSE of 8.11%. In the case that sunshine duration data was unavailable, the model integrating atmospheric constituents with the model suggested by Chen and Li [30] was the most accuracy one with the lowest RMSE of 0.903 MJ m^{-2} and the RRMSE of 8.95%. If all the meteorological variables were available, the model RS15 using all the atmospheric constituents can be used to estimate global solar radiation with reasonable accuracy.

The main novelty of this study is that this is so far the first effort to explore the estimation of global solar radiation combining the MODIS atmospheric products with meteorological variables, and to develop coupled models incorporating the atmospheric constituents into empirical models. Moreover, the most accurate models under different scenarios of data availability were proposed. The results demonstrated that coupling remote sensing with the meteorological variables can enhance the performance of conventional empirical models, which may provide a promising alternative to generate global solar radiation data with better accuracy.

Due to the simplicity, operability and reasonable accuracy, empirical model was the most widely used method in estimating solar radiation. In recent years, many studies investigated the performances of machine learning algorithms such as back-propagation algorithms, extreme learning machines and random forests, and the results showed a great potential in estimating global solar radiation. Thus, it is important for the future works to couple remote sensing with the ground measurements of meteorological variables to estimate solar radiation using machine learning algorithms.

Acknowledgment

The work was supported by Youth Innovation Promotion Association (2018417), National Natural Science Foundation of China (41771460, 41901130, 41701247), Open fund by Jiangsu Key Laboratory of Atmospheric Environment Monitoring and Pollution Control (KHK1806), and Open Fund for Key Laboratory of Mine Geological Disasters and Prevention and Control (2018-08). A Project Funded by the Priority Academic Program Development of Jiangsu Higher Education Institutions (PAPD). We thank the National Meteorological Information Center for providing the long-term meteorological measurements records. We thank NASA Earth Observing System Data and Information System for providing the long-term atmospheric product. Many thanks go to the anonymous reviewers for the comments on the manuscript.

References

[1] Belaid S, Mellit A. Prediction of daily and mean monthly global solar radiation using support vector machine in an arid climate. Energy Convers Manag 2016; 118:105-18.

[2] Wu LF, Huang GMP, Fan JL, Zhang FC, Wang XK, Zeng WZ. Potential of kernel-based nonlinear extension of Arps decline model and gradient boosting with categorical features support for predicting daily global solar radiation in humid regions. Energy Convers Manag 2019; 183: 280-95.

[3] Sun Huaiwei,Gui Dongwei, Yan Baowei.Assessing the potential of random forest method for estimating solar radiation using air pollution index. Energy Convers Manag 2019; 119: 121-9.

[4] Yao Wanxiang, Zhang Chunxiao, Wang Xiao.The research of new daily diffuse solar radiation models modified by air quality index (AQI) in the region with heavy fog and haze. Energy Convers Manag 2017; 139:140-50.

[5] Yao WX, Zhang CX, Wang X, Zhang ZG, Li XL, Di HY. A new correlation between global solar radiation and the quality of sunshine duration in China. Energy Convers Manag 2018; 164:579-87.

[6] Chen JL, Li GS, Wu SJ. Assessing the potential of support vector machine for estimating daily solar radiation using sunshine duration. Energy Convers Manage 2013; 75: 311-18.

[7] Alonso-Montesinos J, Batlles FJ, Bosch JL. Beam, diffuse and global solar irradiance estimation with satellite imagery. Energy Convers Manag 2015; 105:1205-12.

[8] Mahmoudinezhad S, Rezania A, Rosendahl LA. Behavior of hybrid concentrated photovoltaic-thermoelectric generator under variable solar radiation. Energy Convers Manag 2018; 164: 443-52.

[9] Yang ZM, Li WY, Chen XH, Su SH, Lin GX, Chen JC. Maximum efficiency and parametric optimum selection of a concentrated solar spectrum splitting photovoltaic cell-thermoelectric generator system. Energy Convers Manag 2018; 174: 65-71.

[10] Renno C, Petit F, Gatto A. Artificial neural network models for predicting the solar radiation as input of a concentrating photovoltaic system. Energy Convers Manag 2015; 106: 999-1012.

[11] Ismail TM, Ramzy K, Elnaghi BE, Abelwhab MN, El-Salam M. Using MATLAB to model and simulate a photovoltaic system to produce hydrogen. Energy Convers Manag 2019; 185:101-29.

[12] Mousavi SM, Mostafavi ES,Jiao PC. Next generation prediction model for daily solar radiation on horizontal surface using a hybrid neural network and simulated annealing method. Energy Convers Manag 2017; 153: 671-82.

548 [13] Fan JL, Wang XK, Wu LF, Zhou HM, Zhang FC, Yu X, Lu XH, Xiang YZ. Comparison of Support
549 Vector Machine and Extreme Gradient Boosting for predicting daily global solar radiation using
550 temperature and precipitation in humid subtropical climates: A case study in China. Energy
551 Convers Manag 2018; 164: 102-11.
552 [14] Zhou Y, Wang DJ, Liu YF, Liu JP. Diffuse solar radiation models for different climate zones in
553 China: Model evaluation and general model development. Energy Convers Manag 2019; 185:
554 518-36.
555 [15] Alsina EF, Bortolini M, Gamberi M, Regattieri A. Artificial neural network optimization for
556 monthly average daily global solar radiation prediction. Energy Convers Manag 2016; 120: 320-9.
557 [16] Angstrom A. Solar and terrestrial radiation. Q J Roy Meteor Soc 924; 50: 121-6.
558 [17] Prescott JA. Evaporation from a water surface in relation to solar radiation. T Roy Soc South Aust
559 1940; 64: 114-8.
560 [18] Almorox J, Hontoria C. Global solar radiation estimation using sunshine duration in Spain. Energy
561 Convers Manag 2004; 45: 1529-35.
562 [19] Ampratwum DB, Dorvio ASS. Estimation of solar radiation from the number of sunshine hours.
563 Appl Energ 1999; 63: 161-7.
564 [20] Ögelman H, Ecevit A, Tasdemiro E. A new method for estimating solar radiation from bright
565 sunshine data. Sol Energy 1984; 33: 619-25.
566 [21] Bahel V, Bakhsh H, Srinivasan R. A correlation for estimation of global solar radiation. Energy
567 1987; 12:131-5.
568 [22] Newland FJ. A study of solar radiation models for the coastal region of South China. Sol Energy
569 1988; 31: 227-35.

570 [23] Chen JL, He L, Yang H, Ma M, Chen Q, Wu S J, Xiao ZL. Empirical models for estimating
571 monthly global solar radiation: a most comprehensive review and comparative case study in
572 China. Renew Sustain Energy Rev 2019; 108: 91-111.
573 [24] Yorukoglu M, Celik AN. A critical review on the estimation of daily global solar radiation from
574 sunshine duration. Energy Convers. Manage. 2006; 47: 2441-50.
575 [25] Zhou J, Wu YZ, Yan G. General formula for estimation of monthly average daily global solar
576 radiation in China. Energy Convers. Manage. 2005; 46:257-68.
577 [26] Lee Khil-Ha. Improving the correlation between incoming solar radiation and sunshine hour using
578 DTR. Int J Climatol 2015; 35(3): 361-74.
579 [27] Saffaripour MH, Mehrabian MA, Bazargan. Predicting solar radiation fluxes for solar energy
580 system applications. Int J Environ Scu Te 2013; 10(4): 761-8.
581 [28] Bakirci K. Prediction of global solar radiation and comparison with satellite data. J Atmos Sol-Terr
582 Phy 2017; 152: 41-9.
583 [29] Liu JD, Liu JM, Linderholm HW, Chen DL, Yu Q, Wu DG. Observation and calculation of the
584 solar radiation on the Tibetan plateau. Energy Convers Manag 2012: 57(2): 23-32.
585 [30] Chen JL, Li GS. Estimation of monthly average daily solar radiation from measured meteorological
586 data in Yangtze River Basin in China. Int J Climatol 2013; 33: 487-98.
587 [31] Falayi EO, Adepitan JO, Rabiu AB. Empirical models for the correlation of global solar radiation
588 with meteorological data for Iseyin, Nigeria. Int J Phys Sci 2008; 3: 210-6.
589 [32] Ouali K, Alkama R. A new model of global solar radiation based on meteorological data in Bejaia
590 City (Algeria). Energy Procedia 2014; 50: 670-6.

591 [33] Khorasanizadeh H, Mohammadi K, Jalilvand M. A statistical comparative study to demonstrate the
592 merit of day of the year-based models for estimation of horizontal global solar radiation. Energy
593 Convers Manag 2014; 87: 37-47.
594 [34] Hargreaves GH, Samani ZA. Estimating potential evaporation. J Irrig Drain Eng 1982; 108: 225-30.
595 [35] Bristow KL, Campbell GS. On the relationship between incoming solar radiation and daily
596 maximum and minimum temperature. Agr For Meteorol 1984; 31:159-66.
597 [36] Fan J, Chen B, Wu L, Zhang F, Lu X, Xiang Y. Evaluation and development of temperature-based
598 empirical models for estimating daily global solar radiation in humid regions. Energy 2018; 144:
599 903-14.
600 [37] Hunt LA, Kuchar L, Swanton CJ. Estimation of solar radiation for use in crop modeling. Agr For
601 Meteorol 1998; 91: 293-300.
602 [38] Thornton PE, Running SW. An improved algorithm for estimating incident daily solar radiation
603 from measurements of temperature, humidity, and precipitation. Agr For Meteorol 1999; 93:
604 211-28.
605 [39] Ball RA, Purcell LC, Carey SK. Evaluation of Solar radiation prediction models in North America.
606 Agronomy Journal 2004; 96: 391-7.
607 [40] Chen JL, He L, Chen Q, Lv MQ, Zhu HL, Wen ZF, Wu SJ. Study of monthly mean daily diffuse
608 and direct beam radiation estimation with MODIS atmospheric product. Renew Energ 2018; 132:
609 221-32.
610 [41] Bayrakçı HC, Demircan C, Keçebaş A. The development of empirical models for estimating global
611 solar radiation on horizontal surface: a case study. Renew Sustain Energy Rev 2018; 81: 2771-82.

612 [42] Chen JL, Xiao BB, Chen CD, Wen ZF, Jiang Y, Lv MQ, Li GS. Estimation of monthly-mean
613 global solar radiation using MODIS atmospheric product over China. J Atmos Sol-Terr Phy
614 2014; 110: 63-80.
615 [43] Chen JL, Li GS. Parameterization and mapping of solar radiation in data sparse regions. Asia-Pac J
616 Atmos Sci. 2012; 48(4): 423-31.
617 [44] Supit I, Kappel RRV. A simple method to estimate global radiation. Solar Energy 1998; 63, 147-60.
618 [45] Schillings C, Mannstein, H., Meyer, R., 2004. Operational method for deriving high resolution
619 direct normal irradiance from satellite data. Solar Energy, 76, 475-84.
620 [46] Gueymard C. A two-band model for the calculation of clear sky solar irradiance, illuminance, and
621 photosynthetically active radiation at the Earth's surface. Solar Energy 1989; 43: 253-65.
622 [47] Haigh JD. The sun and the earth's climate. Living Rev Sol Phys 2007; 4(1): 2.
623 [48] Levy RC, Mattoo S, Munchak L, Remer LA, Sayer AM, Patadia F, Hsu NC. The Collection 6
624 MODIS aerosol products over land and ocean. Atmospheric Measurement Techniques 2013; 6(11):
625 2989-3034.
626 [49] Liu H, Tang S, Zhang S, Hu J. Evaluation of modis water vapour products over china using
627 radiosonde data. International Journal of Remote Sensing 2015; 36(2): 680-90.
628 [50] Platnick S, Meyer KG, King MD, Wind G, Amarasinghe N, Marchant B. The MODIS cloud optical
629 and microphysical products: Collection 6 updates and examples from Terra and Aqua. IEEE Trans.
630 Geosci. Remote Sens. 2017; 55: 502-25.
631 [51] Ghimire S, Deo RC, Downs NJ, Ra N. Self-adaptive differential evolutionary extreme learning
632 machines for long-term solar radiation prediction with remotely-sensed modis satellite and reanalysis
633 atmospheric products in solar-rich cities. Remote Sensing of Environment 2018; 212, 176-98.

634 [52] Ravinesh CD, Mehmet S. Forecasting long-term global solar radiation with an ANN algorithm
635 coupled with satellite-derived (MODIS) land surface temperature (LST) for regional locations in
636 Queensland. Renew Sustain Energy Rev 72 (2017) 828-48.
637 [53] Zhou Q, Flores A, Glenn NF, Walters R, Han B. A machine learning approach to estimation of
638 downward solar radiation from satellite-derived data products: An application over a semi-arid
639 ecosystem in the U.S. PLoS ONE 2017; 12(8): e0180239.
640 [54] Qin, WM, Wang LC, Lin AW, Zhang M, Xia XG, Hu B, Niu ZG. Comparison of deterministic and
641 data-driven models for solar radiation estimation in China. Renew Sustain Energy Rev 2018;
642 81:579-94.
643 [55] Chen M, Zhuang QL, He YJ. An Efficient Method of Estimating Downward Solar Radiation Based
644 on the MODIS Observations for the Use of Land Surface Modeling. Remote Sens. 2014, 6: 7136-57.
645 [56] Allen RG, Pereira LS, Raes D, Smith M. Crop evapotranspiration guidelines for computing crop
646 water requirements e FAO irrigation and drainage paper 56. Rome: Food and Agriculture
647 Organization of the United Nations; 1998.
648 [57] Bakirci K. Correlations for estimation of daily global solar radiation with hours of bright sunshine
649 in Turkey. Energy 2009; 34(4): 485-501.
650 [58] Olayinka S. Estimation of global and diffuse solar radiations for selected cities in Nigeria. Int J
651 Energy Environ Eng 2011; 3: 13-33.
652 [59] Abdallah YAG. New correlation of global solar radiation with meteorological parameters for
653 Bahrain, Sol Energy 1994; 16:111-20.
654 [60] Swartman RK, Ogunlade O. Solar radiation estimates from common parameters, Sol Energy 1967;
655 11:170-72.

[61] Al-Salihi AM, Kadum MM, Mohammed AJ. Estimation of global solar radiation on horizontal surface using routine meteorological measurements for different cities in Iraq. Asian J Sci Res 2010; 3(4): 240-48.

[62] Chen R, Kang E, Ji X, Yang J, Zhang Z. Trends of the global radiation and sunshine hours in 1961-1998 and their relationships in China. Energy Convers Manag 2006; 47: 2859-66.

[63] Okonkwo GN, Nwokoye AOC. Estimating global solar radiation from temperature data in Minna location. Eur Sci J 2014; 10: 254-64.

[64] Kirmani S, Jamil M, Rizwan M. Empirical correlation of estimating global solar radiation using meteorological parameters. Int J Sustain Energy 2015; 34(5):327-39.

[65] Chen JL, Li GS. Evaluation of support vector machine for estimation of solar radiation from measured meteorological variables. Theor Appl Climatol 2014; 115: 627-38.

[66] Adeala AA, Huan Z, Enweremadu CC. Evaluation of global solar radiation using multiple weather parameters as predictors for South Africa Provinces. Therm Sci 2015; 19: 495-509.

[67] Ouali K, Alkama R. A new model of global solar radiation based on meteorological data in Bejaia City, Algeria. J Sol Energy 2014; 1-9.

[68] Awachie IRN, Okeke CE. New empirical solar model and its use in predicting global solar irradiation. Niger J Sol Energy 1990; 9: 143-56.

[69] Ohunakin OS, Adaramola MS, Oyewolu OM, Fagbenle RO. Correlations for estimating solar radiation using sunshine hours and temperature measurement in OSogbo, Osun state, Nigeria. Front Energy 2013:1-9.

[70] Li MF, Liu HB, Guo PT, Wu W. Estimation of daily solar radiation from routinely observed meteorological data in Chongqing, China. Energy Convers Manage 2010; 51(12):2575-79.

678 [71] Okundamiya MS, Nzeako AN. Estimation of diffuse solar radiation for selected cities in Nigeria.
679 ISRN Renew Energy 2011; 439410.
680 [72] El-Sebaii AA, Al-Ghamdi AA, Al-Hazmi FS, Faidah A. Estimation of global solar radiation on
681 horizontal surfaces in Jeddah, Saudi Arabia. Energy Policy 2009; 37: 3645-49.
682 [73] Korachagaon I, Bapat VN. General formula for the estimation of global solar radiation on earth's
683 surface around the globe. Renew Energ 2012; 41(4): 394-400.
684 [74] Amillo AG, Huld T, Müller R. A New Database of Global and Direct Solar Radiation Using the
685 Eastern Meteosat Satellite, Models and Validation. Remote Sensing 2014; 6: 8165-89.
686 [75] He HP, Wu SJ, Ma MH, Wen ZF, Lv MQ, Chen JL. Spatial distribution and temporal trend of pan
687 evaporation in the three gorges reservoir area and its surroundings during 1952-2013. Appl Ecol Env
688 Res 2017; 15(3):1594-610.
689 [76] King MD, Tsay SC, Platnick SE, Wang M, Liou KN. Cloud Retrieval Algorithms for MODIS:
690 Optical Thickness, Effective Particle Radius, and Thermodynamic Phase. MODIS Algorithm
691 Theoretical Basis Document, ATBD-MOD-05, NASA.1997.
692 [77] Gao BC, Kaufman YJ. The MODIS Near-IR Water Vapor Algorithm. MODIS Algorithm
693 Theoretical Basis Document, ATBD-MOD-03, NASA.1998.
694 [78] Chen JL, Liu HB, Wu W, Xie DT. Estimation of monthly solar radiation from measured
695 temperatures using support vector machines-A case study. Renew Energ 2011; 36(1): 413-20.
696 [79] Liu XY, Mei XR, Li YZ, Wang QS, Jensen JR, Zhang XQ. Evaluation of temperature-based global
697 solar radiation models in China. Agr For Meteorol 2009; 149:1433-46.
698 [80] Stanhill G, Cohen S. Global dimming: a review of the evidence for a widespread and significant
699 reduction in global radiation with discussion of its probable causes and possible agricultural
700 consequences. Agric For Meteorol. 2001; 107: 255-78.

[81] Qin J, Chen Z, Yang K, Liang S, Tang W. Estimation of monthly-mean daily global solar radiation based on MODIS and TRMM products. Appl Energ 2011; 88: 2480-89.

[82] Feng S, Hu Q, Qian W. Quality control of daily meteorological data in China, 1951-2000: a new dataset. Int J Climatol 2004; 24(7): 853-70.

[83] Tang W, Yang K, He J, Qin J. Quality control and estimation of global solar radiation in China. Sol Energy 2010; 84(3): 466-75.

[84] Besharat F, Dehghan AA, Faghih AR. Empirical models for estimating global solar radiation: a review and case study. Renew Sustain Energy Rev 2013; 21(21): 798-821.

[85] Chen RS, Ersi K, Yang JP, Lu SH, Zhao WZ. Validation of five global radiation models with measured daily data in China. Energy Convers Manage 2004; 45:1759-69.

[86] Boluwaji MO, Onyedi DO. Comparative study of ground measured, satellite derived, and estimated global solar radiation data in Nigeria. J Sol Energy 2016; 10: 1-7.

[87] Wu G, Liu Y, Wang T. Methods and strategy for modeling daily global solar radiation with measured meteorological data - a case study in Nanchang station, China. Energy Convers Manag 2007; 48: 2447-52.

[88] Meenal R, Selvakumar AI. Assessment of SVM, empirical and ANN based solar radiation prediction models with most influencing input parameters. Renew Energ 2018; 121: 324-43.

[89] Chen RS, Ersi K, Yang JP, Lu SH, Zhao WZ. Validation of five global radiation models with measured daily data in China. Energy Convers Manage 2004; 45:1759-69.

[90] Iziomon MG, Mayer H. Performance of solar radiation models - a case study. Agric For Meteorol 2001; 10, 1-11.

723 Table 1 Formulas for estimating global solar radiation using atmospheric constituents

Model ID	Equation [a]	RMSE	RRMSE
RS1	$Rs/Ra = a + b_1CF$	1.828	18.12%
RS2	$Rs/Ra = a + b_1COT$	2.237	22.18%
RS3	$Rs/Ra = a + b_1AOT$	2.889	28.64%
RS4	$Rs/Ra = a + b_1PW$	2.387	23.66%
RS5	$Rs/Ra = a + b_1CF + COT$	1.498	14.85%
RS6	$Rs/Ra = a + b_1CF + AOT$	1.815	17.99%
RS7	$Rs/Ra = a + b_1CF + PW$	1.497	14.84%
RS8	$Rs/Ra = a + COT + AOT$	2.147	21.28%
RS9	$Rs/Ra = a + COT + PW$	1.952	19.35%
RS10	$Rs/Ra = a + AOT + PW$	2.391	23.70%
RS11	$Rs/Ra = a + CF + COT + AOT$	1.464	14.52%
RS12	$Rs/Ra = a + CF + COT + PW$	1.269	12.58%
RS13	$Rs/Ra = a + CF + AOT + PW$	1.495	14.82%
RS14	$Rs/Ra = a + COT + AOT + PW$	1.948	19.31%
RS15	$Rs/Ra = a + CF + COT + AOT + PW$	1.267	12.56%

724 [a] Rs, Ra, CF, COT, PWV and AOT are monthly mean global solar radiation, extraterrestrial solar
725 radiation, cloud fraction, cloud optical thickness, precipitable water vapor amount and aerosol optical
726 thickness, respectively.

727

728

729

730

731

732

733

734

735 Table 2 The coupled models incorporating atmospheric constituents into the empirical models

Empirical model	RS1	RS2	RS3	RS4	RS5	RS6	RS7	RS8	RS9	RS10	RS11	RS12	RS13	RS14	RS15
M1	M1RS1	M1RS2	M1RS3	M1RS4	M1RS5	M1RS6	M1RS7	M1RS8	M1RS9	M1RS10	M1RS11	M1RS12	M1RS13	M1RS14	M1RS15
M2	M2RS1	M2RS2	M2RS3	M2RS4	M2RS5	M2RS6	M2RS7	M2RS8	M2RS9	M2RS10	M2RS11	M2RS12	M2RS13	M2RS14	M2RS15
M3	M3RS1	M3RS2	M3RS3	M3RS4	M3RS5	M3RS6	M3RS7	M3RS8	M3RS9	M3RS10	M3RS11	M3RS12	M3RS13	M3RS14	M3RS15
M4	M4RS1	M4RS2	M4RS3	M4RS4	M4RS5	M4RS6	M4RS7	M4RS8	M4RS9	M4RS10	M4RS11	M4RS12	M4RS13	M4RS14	M4RS15
M5	M5RS1	M5RS2	M5RS3	M5RS4	M5RS5	M5RS6	M5RS7	M5RS8	M5RS9	M5RS10	M5RS11	M5RS12	M5RS13	M5RS14	M5RS15
M6	M6RS1	M6RS2	M6RS3	M6RS4	M6RS5	M6RS6	M6RS7	M6RS8	M6RS9	M6RS10	M6RS11	M6RS12	M6RS13	M6RS14	M6RS15
M7	M7RS1	M7RS2	M7RS3	M7RS4	M7RS5	M7RS6	M7RS7	M7RS8	M7RS9	M7RS10	M7RS11	M7RS12	M7RS13	M7RS14	M7RS15
M8	M8RS1	M8RS2	M8RS3	M8RS4	M8RS5	M8RS6	M8RS7	M8RS8	M8RS9	M8RS10	M8RS11	M8RS12	M8RS13	M8RS14	M8RS15
M9	M9RS1	M9RS2	M9RS3	M9RS4	M9RS5	M9RS6	M9RS7	M9RS8	M9RS9	M9RS10	M9RS11	M9RS12	M9RS13	M9RS14	M9RS15
M10	M10RS1	M10RS2	M10RS3	M10RS4	M10RS5	M10RS6	M10RS7	M10RS8	M10RS9	M10RS10	M10RS11	M10RS12	M10RS13	M10RS14	M10RS15
M11	M11RS1	M11RS2	M11RS3	M11RS4	M11RS5	M11RS6	M11RS7	M11RS8	M11RS9	M11RS10	M11RS11	M11RS12	M11RS13	M11RS14	M11RS15
M12	M12RS1	M12RS2	M12RS3	M12RS4	M12RS5	M12RS6	M12RS7	M12RS8	M12RS9	M12RS10	M12RS11	M12RS12	M12RS13	M12RS14	M12RS15
M13	M13RS1	M13RS2	M13RS3	M13RS4	M13RS5	M13RS6	M13RS7	M13RS8	M13RS9	M13RS10	M13RS11	M13RS12	M13RS13	M13RS14	M13RS15
M14	M14RS1	M14RS2	M14RS3	M14RS4	M14RS5	M14RS6	M14RS7	M14RS8	M14RS9	M14RS10	M14RS11	M14RS12	M14RS13	M14RS14	M14RS15
M15	M15RS1	M15RS2	M15RS3	M15RS4	M15RS5	M15RS6	M15RS7	M15RS8	M15RS9	M15RS10	M15RS11	M15RS12	M15RS13	M15RS14	M15RS15
M16	M16RS1	M16RS2	M16RS3	M16RS4	M16RS5	M16RS6	M16RS7	M16RS8	M16RS9	M16RS10	M16RS11	M16RS12	M16RS13	M16RS14	M16RS15
M17	M17RS1	M17RS2	M17RS3	M17RS4	M17RS5	M17RS6	M17RS7	M17RS8	M17RS9	M17RS10	M17RS11	M17RS12	M17RS13	M17RS14	M17RS15
M18	M18RS1	M18RS2	M18RS3	M18RS4	M18RS5	M18RS6	M18RS7	M18RS8	M18RS9	M18RS10	M18RS11	M18RS12	M18RS13	M18RS14	M18RS15
M19	M19RS1	M19RS2	M19RS3	M19RS4	M19RS5	M19RS6	M19RS7	M19RS8	M19RS9	M19RS10	M19RS11	M19RS12	M19RS13	M19RS14	M19RS15
M20	M20RS1	M20RS2	M20RS3	M20RS4	M20RS5	M20RS6	M20RS7	M20RS8	M20RS9	M20RS10	M20RS11	M20RS12	M20RS13	M20RS14	M20RS15
M21	M21RS1	M21RS2	M21RS3	M21RS4	M21RS5	M21RS6	M21RS7	M21RS8	M21RS9	M21RS10	M21RS11	M21RS12	M21RS13	M21RS14	M21RS15
M22	M22RS1	M22RS2	M22RS3	M22RS4	M22RS5	M22RS6	M22RS7	M22RS8	M22RS9	M22RS10	M22RS11	M22RS12	M22RS13	M22RS14	M22RS15

736

737 Table 2 The coupled models incorporating atmospheric constituents into the empirical models (continued)

Empirical model	RS1	RS2	RS3	RS4	RS5	RS6	RS7	RS8	RS9	RS10	RS11	RS12	RS13	RS14	RS15
M23	M23RS1	M23RS2	M23RS3	M23RS4	M23RS5	M23RS6	M23RS7	M23RS8	M23RS9	M23RS10	M23RS11	M23RS12	M23RS13	M23RS14	M23RS15
M24	M24RS1	M24RS2	M24RS3	M24RS4	M24RS5	M24RS6	M24RS7	M24RS8	M24RS9	M24RS10	M24RS11	M24RS12	M24RS13	M24RS14	M24RS15
M25	M25RS1	M25RS2	M25RS3	M25RS4	M25RS5	M25RS6	M25RS7	M25RS8	M25RS9	M25RS10	M25RS11	M25RS12	M25RS13	M25RS14	M25RS15
M26	M26RS1	M26RS2	M26RS3	M26RS4	M26RS5	M26RS6	M26RS7	M26RS8	M26RS9	M26RS10	M26RS11	M26RS12	M26RS13	M26RS14	M26RS15
M27	M27RS1	M27RS2	M27RS3	M27RS4	M27RS5	M27RS6	M27RS7	M27RS8	M27RS9	M27RS10	M27RS11	M27RS12	M27RS13	M27RS14	M27RS15
M28	M28RS1	M28RS2	M28RS3	M28RS4	M28RS5	M28RS6	M28RS7	M28RS8	M28RS9	M28RS10	M28RS11	M28RS12	M28RS13	M28RS14	M28RS15
M29	M29RS1	M29RS2	M29RS3	M29RS4	M29RS5	M29RS6	M29RS7	M29RS8	M29RS9	M29RS10	M29RS11	M29RS12	M29RS13	M29RS14	M29RS15
M30	M30RS1	M30RS2	M30RS3	M30RS4	M30RS5	M30RS6	M30RS7	M30RS8	M30RS9	M30RS10	M30RS11	M30RS12	M30RS13	M30RS14	M30RS15
M31	M31RS1	M31RS2	M31RS3	M31RS4	M31RS5	M31RS6	M31RS7	M31RS8	M31RS9	M31RS10	M31RS11	M31RS12	M31RS13	M31RS14	M31RS15
M32	M32RS1	M32RS2	M32RS3	M32RS4	M32RS5	M32RS6	M32RS7	M32RS8	M32RS9	M32RS10	M32RS11	M32RS12	M32RS13	M32RS14	M32RS15
M33	M33RS1	M33RS2	M33RS3	M33RS4	M33RS5	M33RS6	M33RS7	M33RS8	M33RS9	M33RS10	M33RS11	M33RS12	M33RS13	M33RS14	M33RS15
M34	M34RS1	M34RS2	M34RS3	M34RS4	M34RS5	M34RS6	M34RS7	M34RS8	M34RS9	M34RS10	M34RS11	M34RS12	M34RS13	M34RS14	M34RS15
M35	M35RS1	M35RS2	M35RS3	M35RS4	M35RS5	M35RS6	M35RS7	M35RS8	M35RS9	M35RS10	M35RS11	M35RS12	M35RS13	M35RS14	M35RS15
M36	M36RS1	M36RS2	M36RS3	M36RS4	M36RS5	M36RS6	M36RS7	M36RS8	M36RS9	M36RS10	M36RS11	M36RS12	M36RS13	M36RS14	M36RS15
M37	M37RS1	M37RS2	M37RS3	M37RS4	M37RS5	M37RS6	M37RS7	M37RS8	M37RS9	M37RS10	M37RS11	M37RS12	M37RS13	M37RS14	M37RS15
M38	M38RS1	M38RS2	M38RS3	M38RS4	M38RS5	M38RS6	M38RS7	M38RS8	M38RS9	M38RS10	M38RS11	M38RS12	M38RS13	M38RS14	M38RS15
M39	M39RS1	M39RS2	M39RS3	M39RS4	M39RS5	M39RS6	M39RS7	M39RS8	M39RS9	M39RS10	M39RS11	M39RS12	M39RS13	M39RS14	M39RS15
M40	M40RS1	M40RS2	M40RS3	M40RS4	M40RS5	M40RS6	M40RS7	M40RS8	M40RS9	M40RS10	M40RS11	M40RS12	M40RS13	M40RS14	M40RS15
M41	M41RS1	M41RS2	M41RS3	M41RS4	M41RS5	M41RS6	M41RS7	M41RS8	M41RS9	M41RS10	M41RS11	M41RS12	M41RS13	M41RS14	M41RS15
M42	M42RS1	M42RS2	M42RS3	M42RS4	M42RS5	M42RS6	M42RS7	M42RS8	M42RS9	M42RS10	M42RS11	M42RS12	M42RS13	M42RS14	M42RS15
M43	M43RS1	M43RS2	M43RS3	M43RS4	M43RS5	M43RS6	M43RS7	M43RS8	M43RS9	M43RS10	M43RS11	M43RS12	M43RS13	M43RS14	M43RS15

738

739

740 Table 3 Performance of the collected empirical models

Empirical model	RMSE	RRMSE	Empirical model	RMSE	RRMSE
Model 1	1.129	11.19%	Model 26	1.621	16.07%
Model 2	1.129	11.19%	Model 27	1.94	19.23%
Model 3	1.128	11.18%	Model 28	2.099	20.81%
Model 4	1.129	11.19%	Model 29	1.801	17.86%
Model 5	1.127	11.18%	Model 30	1.532	15.19%
Model 6	1.041	10.32%	Model 31	1.523	15.10%
Model 7	1.05	10.41%	Model 32	1.796	17.81%
Model 8	1.031	10.22%	Model 33	1.404	13.92%
Model 9	1.015	10.07%	Model 34	1.315	13.04%
Model 10	1.124	11.14%	Model 35	1.981	19.64%
Model 11	1.055	10.46%	Model 36	1.631	16.17%
Model 12	0.969	9.60%	Model 37	1.31	12.98%
Model 13	0.997	9.89%	Model 38	1.471	14.58%
Model 14	1.077	10.68%	Model 39	1.612	15.98%
Model 15	0.98	9.71%	Model 40	1.581	15.67%
Model 16	1.067	10.58%	Model 41	1.37	13.59%
Model 17	1.113	11.03%	Model 42	1.154	11.44%
Model 18	1.111	11.02%	Model 43	1.194	11.84%
Model 19	0.972	9.64%			
Model 20	1.028	10.19%			
Model 21	1.04	10.31%			
Model 22	0.979	9.70%			
Model 23	1.012	10.03%			
Model 24	0.968	9.60%			
Model 25	0.967	9.58%			

741 Table 4 The RMSE (MJ m^{-2}) of the coupled models

Empirical model	RS1	RS2	RS3	RS4	RS5	RS6	RS7	RS8	RS9	RS10	RS11	RS12	RS13	RS14	RS15
Model 1	1.108	1.011	1.129	1.064	0.984	1.110	1.026	1.012	0.954	1.050	0.986	0.909	1.012	0.950	0.904
Model 2	1.107	1.003	1.129	1.063	0.969	1.109	1.026	1.004	0.953	1.047	0.969	0.902	1.011	0.949	0.899
Model 3	1.106	1.004	1.129	1.064	0.973	1.108	1.026	1.005	0.953	1.048	0.973	0.904	1.012	0.949	0.901
Model 4	1.107	1.003	1.129	1.063	0.968	1.109	1.027	1.003	0.952	1.047	0.968	0.902	1.011	0.949	0.899
Model 5	1.106	0.999	1.128	1.063	0.965	1.107	1.027	1.000	0.952	1.047	0.965	0.901	1.012	0.948	0.899
Model 6	1.005	0.910	1.023	1.038	0.863	0.988	1.005	0.901	0.885	1.021	0.855	0.845	0.987	0.879	0.838
Model 7	1.014	0.918	1.030	1.050	0.869	0.994	1.014	0.907	0.899	1.030	0.859	0.855	0.994	0.888	0.845
Model 8	0.996	0.899	1.017	1.027	0.852	0.982	0.995	0.893	0.873	1.015	0.847	0.834	0.982	0.871	0.832
Model 9	0.987	0.884	1.011	1.015	0.844	0.982	0.986	0.884	0.873	1.011	0.843	0.835	0.981	0.872	0.833
Model 10	1.099	0.988	1.122	1.06	0.949	1.098	1.024	0.988	0.953	1.048	0.949	0.905	1.011	0.948	0.899
Model 11	1.009	0.947	1.048	1.051	0.894	1.002	1.006	0.946	0.944	1.04	0.893	0.891	0.995	0.941	0.888
Model 12	0.923	0.874	0.969	0.967	0.824	0.923	0.917	0.874	0.867	0.967	0.824	0.821	0.917	0.867	0.821
Model 13	0.974	0.882	0.996	0.997	0.844	0.972	0.973	0.881	0.871	0.996	0.843	0.835	0.971	0.87	0.833
Model 14	1.062	0.962	1.076	1.021	0.942	1.06	0.992	0.954	0.912	1.02	0.932	0.874	0.989	0.912	0.874
Model 15	0.927	0.892	0.977	0.98	0.834	0.926	0.925	0.889	0.877	0.977	0.833	0.828	0.924	0.874	0.826
Model 16	1.049	0.962	1.06	0.974	0.942	1.04	0.924	0.954	0.903	0.973	0.931	0.855	0.923	0.901	0.853
Model 17	1.089	1.01	1.115	1.002	0.984	1.091	0.942	1.012	0.937	1.001	0.985	0.879	0.942	0.937	0.879
Model 18	1.083	1.002	1.113	1.002	0.965	1.083	0.937	1.002	0.933	1.001	0.962	0.864	0.937	0.933	0.864
Model 19	0.921	0.882	0.971	0.972	0.826	0.921	0.92	0.881	0.867	0.971	0.826	0.82	0.919	0.867	0.82
Model 20	0.997	0.909	1.014	1.025	0.863	0.983	0.996	0.901	0.884	1.012	0.854	0.845	0.982	0.878	0.838
Model 21	1.008	0.917	1.023	1.04	0.869	0.99	1.008	0.907	0.899	1.023	0.859	0.855	0.99	0.888	0.844
Model 22	0.927	0.892	0.976	0.979	0.831	0.926	0.925	0.889	0.877	0.976	0.83	0.826	0.924	0.874	0.824

742 Table 4 The RMSE (MJ m^{-2}) of the coupled models (continued)

Empirical model	RS1	RS2	RS3	RS4	RS5	RS6	RS7	RS8	RS9	RS10	RS11	RS12	RS13	RS14	RS15
Model 23	0.954	0.930	1.011	0.977	0.877	0.954	0.922	0.928	0.905	0.976	0.875	0.854	0.921	0.903	0.852
Model 24	0.920	0.882	0.968	0.968	0.829	0.920	0.919	0.882	0.866	0.968	0.829	0.822	0.919	0.866	0.821
Model 25	0.920	0.882	0.968	0.968	0.825	0.920	0.918	0.881	0.866	0.968	0.825	0.818	0.918	0.865	0.817
Model 26	1.409	1.423	1.514	1.521	1.225	1.344	1.278	1.296	1.344	1.472	1.140	1.112	1.263	1.275	1.084
Model 27	1.410	1.593	1.925	1.662	1.165	1.397	1.351	1.591	1.269	1.653	1.162	1.054	1.340	1.268	1.052
Model 28	1.469	1.702	2.086	1.917	1.208	1.454	1.441	1.7	1.437	1.899	1.203	1.122	1.424	1.434	1.117
Model 29	1.353	1.489	1.791	1.529	1.118	1.344	1.287	1.488	1.188	1.528	1.116	1.01	1.284	1.185	1.01
Model 30	1.407	1.391	1.445	1.404	1.227	1.341	1.28	1.274	1.299	1.379	1.141	1.118	1.264	1.245	1.089
Model 31	1.393	1.362	1.434	1.379	1.222	1.329	1.241	1.249	1.242	1.355	1.137	1.093	1.231	1.199	1.07
Model 32	1.337	1.592	1.742	1.381	1.165	1.296	1.201	1.587	1.228	1.319	1.162	1.043	1.15	1.214	1.035
Model 33	1.223	1.212	1.381	1.392	1.03	1.219	1.221	1.181	1.155	1.374	1.021	1.001	1.218	1.136	0.996
Model 34	1.182	1.177	1.283	1.306	1.022	1.173	1.181	1.14	1.129	1.279	1.011	0.995	1.172	1.104	0.988
Model 35	1.394	1.699	1.935	1.648	1.206	1.354	1.303	1.699	1.42	1.563	1.203	1.118	1.238	1.404	1.105
Model 36	1.273	1.475	1.576	1.225	1.117	1.235	1.118	1.466	1.108	1.189	1.114	0.983	1.085	1.102	0.98
Model 37	1.054	1.239	1.303	1.279	0.971	1.053	1.054	1.231	1.231	1.152	1.274	0.969	0.952	1.052	1.148
Model 38	1.293	1.368	1.308	1.259	1.188	1.182	1.045	1.204	1.206	1.19	1.073	0.99	1.016	1.127	0.954
Model 39	1.41	1.424	1.473	1.449	1.21	1.338	1.251	1.288	1.325	1.378	1.14	1.111	1.226	1.244	1.08
Model 40	1.309	1.396	1.508	1.509	1.143	1.291	1.278	1.297	1.328	1.455	1.109	1.112	1.264	1.251	1.084
Model 41	1.114	1.299	1.269	1.248	1.05	1.078	1.044	1.186	1.194	1.173	1.005	0.99	1.016	1.107	0.954
Model 42	1.024	1.028	1.125	1.154	0.919	1.012	1.021	0.998	1.017	1.122	0.905	0.915	1.006	0.993	0.903
Model 43	1.469	1.702	2.086	1.917	1.208	1.454	1.441	1.7	1.437	1.899	1.203	1.122	1.424	1.434	1.117

743

744 Table 5 The RRMSE of the coupled models

Empirical model	RS1	RS2	RS3	RS4	RS5	RS6	RS7	RS8	RS9	RS10	RS11	RS12	RS13	RS14	RS15
Model 1	10.99%	10.02%	11.20%	10.55%	9.76%	11.00%	10.17%	10.03%	9.46%	10.41%	9.77%	9.01%	10.03%	9.41%	8.97%
Model 2	10.98%	9.94%	11.20%	10.53%	9.60%	10.99%	10.18%	9.95%	9.44%	10.38%	9.61%	8.94%	10.03%	9.40%	8.91%
Model 3	10.96%	9.96%	11.19%	10.55%	9.64%	10.98%	10.18%	9.97%	9.45%	10.39%	9.65%	8.96%	10.03%	9.41%	8.94%
Model 4	10.98%	9.94%	11.20%	10.54%	9.60%	10.99%	10.18%	9.95%	9.44%	10.38%	9.60%	8.94%	10.03%	9.40%	8.91%
Model 5	10.96%	9.91%	11.18%	10.54%	9.57%	10.98%	10.18%	9.91%	9.43%	10.38%	9.57%	8.94%	10.03%	9.40%	8.91%
Model 6	9.97%	9.02%	10.14%	10.29%	8.55%	9.79%	9.96%	8.93%	8.77%	10.12%	8.47%	8.37%	9.79%	8.71%	8.31%
Model 7	10.05%	9.10%	10.21%	10.41%	8.62%	9.85%	10.05%	9.00%	8.91%	10.21%	8.52%	8.47%	9.85%	8.81%	8.37%
Model 8	9.87%	8.91%	10.08%	10.18%	8.45%	9.73%	9.86%	8.85%	8.65%	10.06%	8.39%	8.27%	9.74%	8.64%	8.25%
Model 9	9.79%	8.77%	10.03%	10.06%	8.37%	9.73%	9.78%	8.76%	8.65%	10.03%	8.36%	8.28%	9.73%	8.64%	8.26%
Model 10	10.90%	9.79%	11.13%	10.51%	9.41%	10.88%	10.16%	9.79%	9.45%	10.39%	9.41%	8.97%	10.03%	9.40%	8.92%
Model 11	10.00%	9.39%	10.39%	10.42%	8.87%	9.93%	9.98%	9.38%	9.36%	10.31%	8.85%	8.83%	9.86%	9.33%	8.80%
Model 12	9.15%	8.66%	9.60%	9.58%	8.17%	9.15%	9.10%	8.66%	8.59%	9.58%	8.17%	8.14%	9.10%	8.59%	8.14%
Model 13	9.66%	8.74%	9.87%	9.88%	8.36%	9.63%	9.65%	8.74%	8.63%	9.87%	8.35%	8.27%	9.63%	8.62%	8.26%
Model 14	10.53%	9.54%	10.66%	10.12%	9.33%	10.51%	9.83%	9.45%	9.04%	10.11%	9.24%	8.67%	9.81%	9.04%	8.67%
Model 15	9.19%	8.84%	9.69%	9.71%	8.27%	9.18%	9.17%	8.81%	8.69%	9.69%	8.26%	8.20%	9.16%	8.67%	8.19%
Model 16	10.40%	9.54%	10.51%	9.66%	9.33%	10.31%	9.16%	9.45%	8.95%	9.65%	9.23%	8.47%	9.15%	8.93%	8.46%
Model 17	10.80%	10.02%	11.06%	9.93%	9.75%	10.81%	9.34%	10.03%	9.29%	9.93%	9.76%	8.71%	9.34%	9.29%	8.71%
Model 18	10.74%	9.93%	11.03%	9.93%	9.57%	10.74%	9.29%	9.93%	9.25%	9.92%	9.54%	8.57%	9.29%	9.25%	8.57%
Model 19	9.13%	8.74%	9.63%	9.64%	8.19%	9.13%	9.12%	8.73%	8.60%	9.63%	8.19%	8.13%	9.11%	8.59%	8.13%
Model 20	9.89%	9.01%	10.05%	10.16%	8.55%	9.74%	9.88%	8.93%	8.76%	10.03%	8.47%	8.37%	9.74%	8.71%	8.31%
Model 21	9.99%	9.09%	10.14%	10.31%	8.62%	9.82%	9.99%	9.00%	8.91%	10.14%	8.52%	8.47%	9.82%	8.81%	8.37%
Model 22	9.19%	8.84%	9.68%	9.70%	8.24%	9.18%	9.17%	8.81%	8.69%	9.68%	8.23%	8.18%	9.16%	8.67%	8.17%

745 Table 5 The RRMSE of the coupled models (continued)

Empirical model	RS1	RS2	RS3	RS4	RS5	RS6	RS7	RS8	RS9	RS10	RS11	RS12	RS13	RS14	RS15
Model 23	9.46%	9.22%	10.02%	9.68%	8.69%	9.46%	9.14%	9.20%	8.98%	9.67%	8.68%	8.46%	9.13%	8.95%	8.45%
Model 24	9.12%	8.75%	9.60%	9.60%	8.22%	9.12%	9.11%	8.74%	8.59%	9.60%	8.22%	8.14%	9.11%	8.58%	8.14%
Model 25	9.12%	8.74%	9.59%	9.59%	8.18%	9.12%	9.10%	8.74%	8.58%	9.59%	8.18%	8.11%	9.11%	8.58%	8.10%
Model 26	13.97%	14.11%	15.01%	15.08%	12.14%	13.32%	12.67%	12.85%	13.33%	14.59%	11.30%	11.02%	12.53%	12.64%	10.75%
Model 27	13.98%	15.79%	19.08%	16.47%	11.55%	13.85%	13.40%	15.77%	12.58%	16.38%	11.52%	10.44%	13.29%	12.57%	10.43%
Model 28	14.57%	16.87%	20.68%	19.00%	11.97%	14.42%	14.29%	16.85%	14.25%	18.82%	11.93%	11.12%	14.12%	14.22%	11.08%
Model 29	13.42%	14.76%	17.75%	15.16%	11.08%	13.32%	12.76%	14.75%	11.78%	15.15%	11.06%	10.01%	12.73%	11.75%	10.01%
Model 30	13.95%	13.79%	14.32%	13.92%	12.17%	13.30%	12.69%	12.63%	12.88%	13.67%	11.31%	11.08%	12.54%	12.34%	10.79%
Model 31	13.81%	13.50%	14.22%	13.67%	12.11%	13.18%	12.30%	12.39%	12.31%	13.43%	11.27%	10.84%	12.20%	11.89%	10.61%
Model 32	13.25%	15.78%	17.27%	13.69%	11.55%	12.85%	11.91%	15.73%	12.17%	13.08%	11.52%	10.34%	11.41%	12.04%	10.26%
Model 33	12.12%	12.02%	13.69%	13.80%	10.21%	12.08%	12.11%	11.71%	11.45%	13.63%	10.12%	9.92%	12.07%	11.26%	9.87%
Model 34	11.72%	11.67%	12.72%	12.94%	10.14%	11.63%	11.71%	11.30%	11.19%	12.68%	10.02%	9.86%	11.62%	10.95%	9.80%
Model 35	13.82%	16.85%	19.18%	16.34%	11.96%	13.42%	12.92%	16.84%	14.08%	15.49%	11.93%	11.08%	12.27%	13.91%	10.96%
Model 36	12.62%	14.63%	15.62%	12.14%	11.08%	12.24%	11.08%	14.53%	10.99%	11.79%	11.04%	9.75%	10.76%	10.93%	9.72%
Model 37	10.45%	12.28%	12.92%	12.68%	9.63%	10.44%	10.45%	12.20%	12.20%	11.42%	12.63%	9.60%	9.44%	10.43%	11.38%
Model 38	12.82%	13.56%	12.97%	12.48%	11.78%	11.71%	10.36%	11.93%	11.96%	11.80%	10.64%	9.82%	10.07%	11.17%	9.46%
Model 39	13.98%	14.11%	14.61%	14.37%	11.99%	13.27%	12.40%	12.77%	13.13%	13.67%	11.30%	11.01%	12.15%	12.33%	10.70%
Model 40	12.97%	13.84%	14.95%	14.96%	11.33%	12.80%	12.67%	12.86%	13.16%	14.43%	10.99%	11.02%	12.53%	12.40%	10.75%
Model 41	11.04%	12.88%	12.59%	12.37%	10.41%	10.69%	10.35%	11.76%	11.84%	11.63%	9.96%	9.82%	10.07%	10.98%	9.46%
Model 42	10.15%	10.19%	11.16%	11.44%	9.11%	10.04%	10.12%	9.89%	10.08%	11.12%	8.97%	9.07%	9.98%	9.84%	8.95%
Model 43	10.16%	11.00%	11.48%	11.83%	9.26%	10.05%	10.14%	10.60%	10.80%	11.48%	9.11%	9.21%	9.99%	10.50%	9.09%

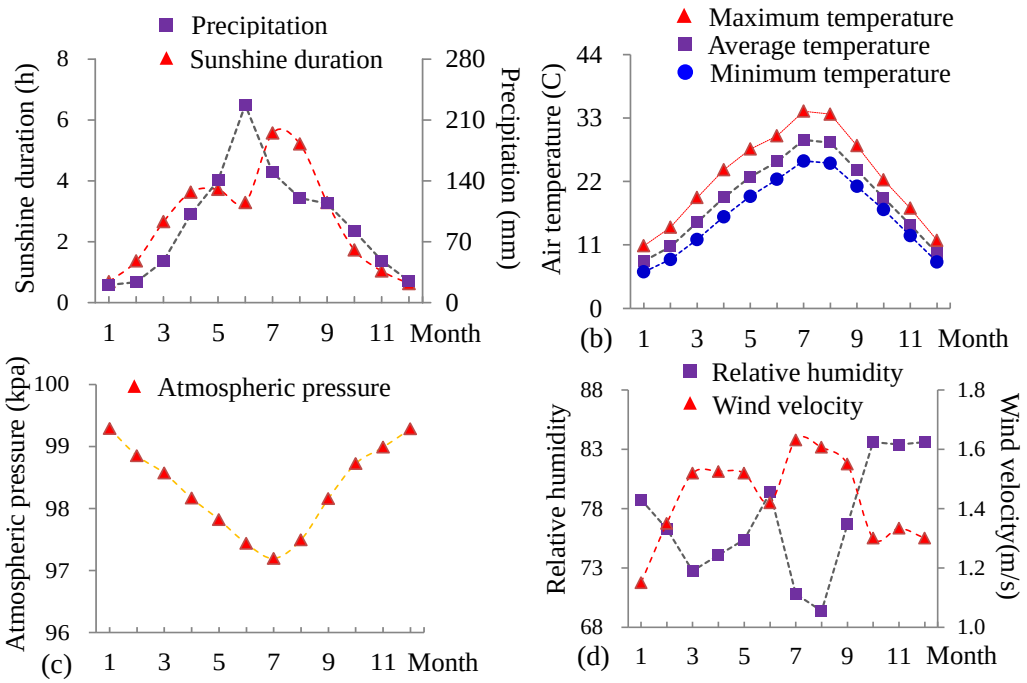

746

747 Figure.1 Temporal variations of the meteorological variables in Chongqing, China

748